doi:10.1093/brain/awx339 BRAIN 2018: 141; 459–471 | 459

BRAIN
A JOURNAL OF NEUROLOGY

Minocycline reduces chronic microglial activation after brain trauma but increases neurodegeneration

Gregory Scott,[1] Henrik Zetterberg,[2,3,4] Amy Jolly,[1] James H. Cole,[1] Sara De Simoni,[1] Peter O. Jenkins,[1] Claire Feeney,[1] David R. Owen,[1] Anne Lingford-Hughes,[1] Oliver Howes,[1] Maneesh C. Patel,[5] Anthony P. Goldstone,[1] Roger N. Gunn,[6] Kaj Blennow,[2,3] Paul M. Matthews[1] and David J. Sharp[1]

Survivors of a traumatic brain injury can deteriorate years later, developing brain atrophy and dementia. Traumatic brain injury triggers chronic microglial activation, but it is unclear whether this is harmful or beneficial. A successful chronic-phase treatment for traumatic brain injury might be to target microglia. In experimental models, the antibiotic minocycline inhibits microglial activation. We investigated the effect of minocycline on microglial activation and neurodegeneration using PET, MRI, and measurement of the axonal protein neurofilament light in plasma. Microglial activation was assessed using ^{11}C-PBR28 PET. The relationships of microglial activation to measures of brain injury, and the effects of minocycline on disease progression, were assessed using structural and diffusion MRI, plasma neurofilament light, and cognitive assessment. Fifteen patients at least 6 months after a moderate-to-severe traumatic brain injury received either minocycline 100 mg orally twice daily or no drug, for 12 weeks. At baseline, ^{11}C-PBR28 binding in patients was increased compared to controls in cerebral white matter and thalamus, and plasma neurofilament light levels were elevated. MRI measures of white matter damage were highest in areas of greater ^{11}C-PBR28 binding. Minocycline reduced ^{11}C-PBR28 binding (mean Δwhite matter binding = −23.30%, 95% confidence interval −40.9 to −5.64%, $P = 0.018$), but increased plasma neurofilament light levels. Faster rates of brain atrophy were found in patients with higher baseline neurofilament light levels. In this experimental medicine study, minocycline after traumatic brain injury reduced chronic microglial activation while increasing a marker of neurodegeneration. These findings suggest that microglial activation has a reparative effect in the chronic phase of traumatic brain injury.

1 Division of Brain Sciences, Department of Medicine, Imperial College London, UK
2 Department of Psychiatry and Neurochemistry, Institute of Neuroscience and Physiology, the Sahlgrenska Academy at the University of Gothenburg, Mölndal, Sweden
3 Clinical Neurochemistry Laboratory, Sahlgrenska University Hospital, Mölndal, Sweden
4 Department of Molecular Neuroscience, UCL Institute of Neurology, London, UK
5 Charing Cross Hospital, Imperial College Healthcare NHS Trust, London, UK
6 Imanova Ltd, London, UK

Correspondence to: Prof David J. Sharp
Computational, Cognitive and Clinical Neuroimaging Laboratory, 3rd Floor, Burlington Danes Building, Imperial College London, Hammersmith Hospital, Du Cane Road, London, W12 0NN, UK
E-mail: david.sharp@imperial.ac.uk

Keywords: traumatic brain injury; microglia; minocycline; neurodegeneration; positron emission tomography

Abbreviations: CMA = chronic microglial activation; DVR = distribution volume ratio; NFL = neurofilament light chain; TBI = traumatic brain injury; V_T = volume of distribution

Received July 2, 2017. Revised September 20, 2017. Accepted October 19, 2017. Advance Access publication December 19, 2017

Introduction

Survivors of traumatic brain injury (TBI) can deteriorate years after injury (Whitnall *et al.*, 2006), developing post-traumatic epilepsy (Annegers *et al.*, 1998), brain atrophy (Cole *et al.*, 2015), Alzheimer's disease (Smith *et al.*, 2013) and chronic traumatic encephalopathy (CTE) (McKee *et al.*, 2013). The protracted effects of TBI suggest a window of opportunity for disease-modifying therapy that extends beyond the acute setting, where many clinical trials have failed (Maas *et al.*, 2004).

The long-term clinical effects of TBI are associated with chronic microglial activation (CMA) (Ramlackhansingh *et al.*, 2011) and progressive neurodegeneration (Sidaros *et al.*, 2009), both of which are seen in white matter tracts affected by the injury (Johnson *et al.*, 2013). Animal models (Loane *et al.*, 2014), neuropathology (Johnson *et al.*, 2013), and molecular imaging (Ramlackhansingh *et al.*, 2011) show that CMA can persist for years after TBI. However, its significance is unclear (Ransohoff, 2016). Microglia are implicated in the pathogenesis of many neurodegenerative diseases (Gentleman, 2013). In rodent TBI models, microglia have a predominantly pro-inflammatory activation phenotype (Loane *et al.*, 2014). However, studies in non-human primates in the chronic phase suggest a reparative role (Nagamoto-Combs *et al.*, 2007, 2010).

PET ligands targeting the translocator protein (TSPO), upregulated in activated microglia, can be used to quantify CMA *in vivo* (Raghavendra Rao *et al.*, 2000). We previously demonstrated CMA up to 17 years after TBI using the TSPO ligand ^{11}C-PK11195 (Ramlackhansingh *et al.*, 2011). Second-generation TSPO ligands, including ^{11}C-PBR28 (Owen *et al.*, 2014), have a higher signal-to-noise ratio, promising more accurate quantification.

A successful treatment strategy for TBI might be to target CMA. The antibiotic minocycline has anti-inflammatory properties and is neuroprotective in models of TBI (Siopi *et al.*, 2011) and other neurological disorders (Plane *et al.*, 2010). One mechanism of action is the inhibition of microglial activation (Homsi *et al.*, 2010). In models of acute TBI, minocycline reduces microglial activation and improves early functional outcomes (Siopi *et al.*, 2011). Clinical trials in acute stroke and spinal cord injury have shown positive results (Lampl *et al.*, 2007; Casha *et al.*, 2012). However, trials in neurodegenerative diseases have had mixed results (Plane *et al.*, 2010): the largest trial, in amyotrophic lateral sclerosis (ALS), reported a negative effect on functional outcomes (Gordon *et al.*, 2007).

We examined the role of CMA in TBI and the effects of minocycline on microglia and neurodegeneration. We hypothesized that: (i) levels of CMA predict subsequent neurodegeneration; (ii) minocycline reduces CMA; and (iii) inhibiting CMA reduces neurodegeneration. To test these hypotheses, we combined ^{11}C-PBR28 PET with MRI measures of neurodegeneration (atrophy) and measurement of plasma neurofilament light chain (NFL), a marker of axonal injury (Ljungqvist *et al.*, 2017) and active neurodegeneration (Bacioglu *et al.*, 2016*a*).

Materials and methods

Experimental design

We undertook a cross-sectional study of TBI patients compared to controls, followed by a randomized open-label study of minocycline versus no drug in patients (Fig. 1). ^{11}C-PBR28 PET, MRI, plasma NFL measurement and cognitive testing were performed at baseline. Patients were then randomized to one of two arms (2:1 ratio), balanced for age, gender, *TSPO* genotype and time since injury. One group ($n = 10$) received minocycline 100 mg orally twice daily for 12 weeks; the other ($n = 5$) had no drug. Patients were followed up at 12 weeks (^{11}C-PBR28 PET, MRI, NFL and cognitive testing) and 6 months (MRI, NFL, cognitive testing). The study was approved by the West London and GTAC NHS Research Ethics Committee (13/LO/1813). All participants provided informed consent.

Participants

Patients were recruited from TBI clinics in London, UK. Inclusion criteria were: age between 20–65 years; history of a single moderate-severe TBI (Mayo classification) (Malec *et al.*, 2007) at least 6 months prior; no significant neurological or psychiatric illness prior to the TBI. Exclusion criteria were: use of any medication, substance or alcohol abuse that would interfere with the study or compromise safety; contraindication to MRI scanning; contraindication to PET or arterial line insertion. Three separate groups of healthy controls, age- and gender-matched to the TBI group, were used (Table 1 and Fig. 1). Screening included genotyping for the rs6971 (Ala147Thr) polymorphism in the *TSPO* gene. This produces three classes of binding affinity for TSPO: high-, mixed- and low-affinity binders (Owen *et al.*, 2012). Low-affinity binders were excluded as they show negligible specific binding of ^{11}C-PBR28. PET controls were matched to patients for *TSPO* genotype.

Procedures

Study procedures were carried out at the Hammersmith Hospital campus, Imperial College London (London, UK) and Imanova Centre for Imaging Sciences (London, UK). ^{11}C-PBR28 radiopharmaceutical preparation and quality control were performed as in Owen *et al.* (2014). ^{11}C-PBR28 was injected as an intravenous bolus [mean ± standard deviation (SD) 340.04 ± 18.07 MBq] over ~20 s at the start of a 90 min dynamic PET acquisition. Radial artery blood samples were collected for generation of an arterial plasma input function. Acquisition and reconstruction of PET imaging data, arterial blood sampling, analysis of plasma metabolism, and measurement of blood and plasma radioactivity concentrations were performed as previously described (Owen *et al.*, 2014).

All participants underwent high resolution T_1 MRI. Diffusion-weighted images were acquired along 64 non-colinear directions

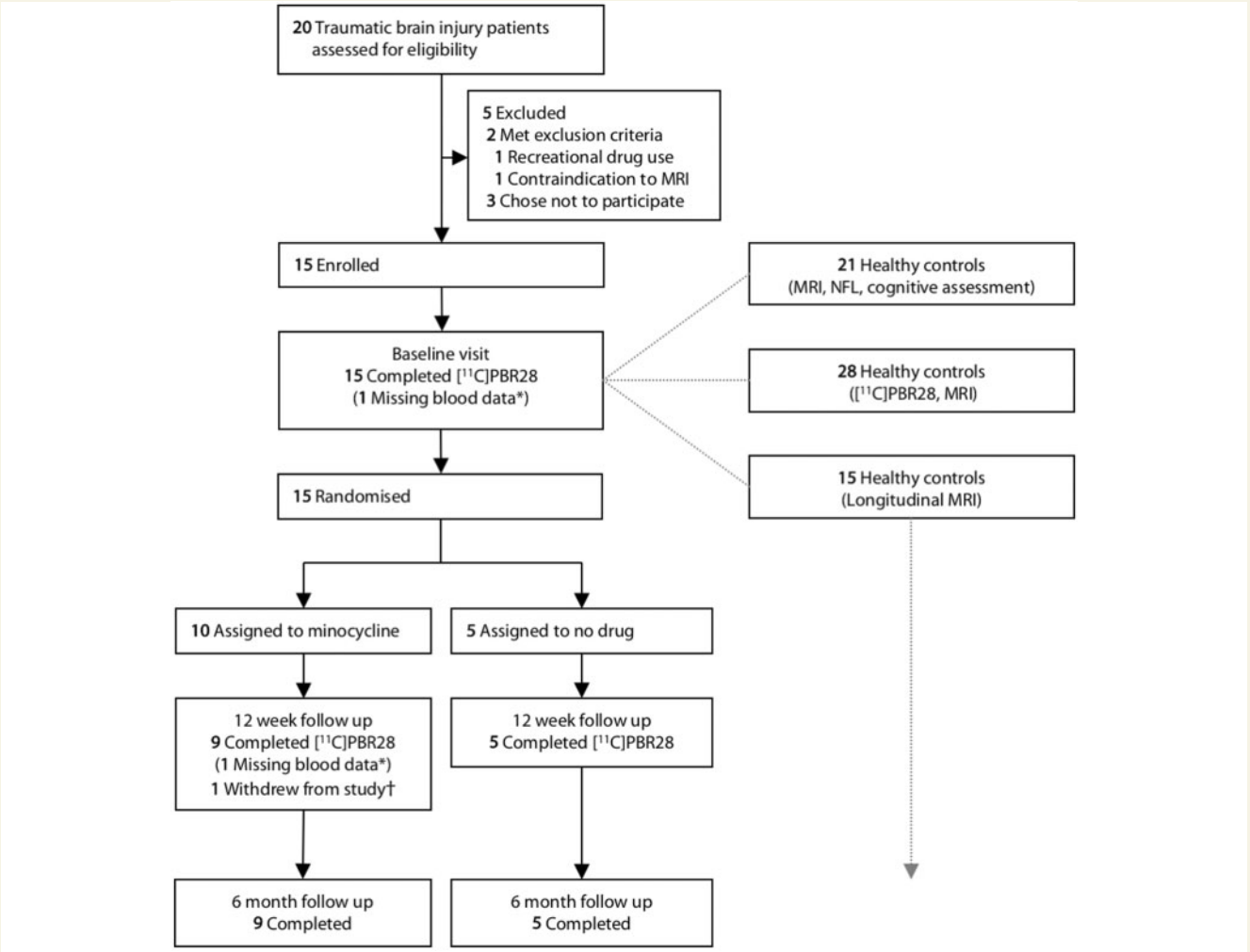

Figure 1 Study design, TBI enrolment and control groups. Baseline data in TBI patients were compared to two control groups, and longitudinal MRI data in patients were compared to a third control group (Table 1). *Arterial blood sampling in two patients in the minocycline group failed (one baseline visit, one 12-week visit), so within-subject comparisons of PET data for these participants were not possible. †A third patient in the minocycline group had an anxiety episode at the start of the 12-week scan and immediately withdrew from the study, so all follow-up data from this participant were excluded.

Table 1 Baseline group demographics

Group	*n*	Age, years, mean ± SD (min–max)	*P*-value	Gender, *n* male (%)	*P*-value	HABs, *n* (%)	*P*-value
TBI	15	42.3 ± 13.7 years (23–61)	-	13 (87)	-	9 (60)	-
Control 1 (^{11}C-PBR28 PET)	28	40.8 ± 14.8 years (21–63)	0.756	23 (82)	0.532	16 (57.1)	0.559
Control 2 (MRI, NFL, cognitive assessment)	21	41.6 ± 11.8 years (21–61)	0.881	17 (81)	0.507	-	-
Control 3 (Longitudinal MRI)	15	36.2 ± 8.9 years (27–65)	0.168	12 (80)	0.500	-	-

P-values denote comparisons with the TBI group. HABs = high-affinity binders; SD = standard deviation.

with b = 1000 s/mm^2 and four averages with b = 0 s/mm^2, with echo time/repetition time 103/9500 ms, 64 contiguous slices, field of view 256 mm, and voxel size 2 × 2 × 2 mm^3. Baseline structural MRI scans were reviewed by a senior neuroradiologist.

A neuropsychological battery assessed cognitive domains often previously observed to be impaired after TBI (Supplementary Table 2), as in Ramlackhansingh *et al.* (2011). A venous blood sample was taken on the morning of the 12-week visit for a trough drug level. Plasma concentrations of minocycline were determined using liquid chromatography–mass spectrometry (Antimicrobial Reference Laboratory, Southmead Hospital, Bristol). Venous blood samples were taken for measurement of NFL using the highly-sensitive single molecule array platform

(Simoa; Quanterix Corp) (Kuhle *et al.*, 2016). All analyses were performed on one round of experiments using one batch of reagents by board-certified laboratory technicians who were blinded to clinical data.

PET analysis

Motion correction of dynamic PET images, co-registration of PET with structural MRI, and generation of metabolite-corrected plasma input function were performed using previously published methods (Owen *et al.*, 2014) (Supplementary Fig. 1). The Logan graphical method (Logan *et al.*, 1990), using a metabolite-corrected plasma input function, 5% fixed blood volume and a linear start time (T*) at 35 min, was used to generate parametric maps of volume of distribution (V_T).

^{11}C-PBR28 V_T was the primary outcome measure for assessing within-subject drug effects. As in previous studies (Loggia *et al.*, 2015), ^{11}C-PBR28 distribution volume ratio (DVR), the ratio of regional V_T to whole brain V_T, was used as the primary outcome measure for cross-sectional PET analysis to reduce between-subject variability. Analyses were repeated using cerebellar or cortical grey matter as alternative pseudo-reference regions, to determine if the choice of reference region influenced the findings.

T_1 MRI images were segmented into grey matter and white matter using SPM12, and warped to an average group template using a diffeomorphic non-linear registration (DARTEL) (Ashburner, 2007) (Supplementary Fig. 1A). Separate templates were created for cross-sectional and longitudinal analyses. Templates were registered to Montreal Neurological Institute (MNI) 152 space. Each individual ^{11}C-PBR28 parametric map (DVR or V_T) was registered to its corresponding subject-space T_1, then the individual flow-fields and template transformation from DARTEL were applied to produce MNI space images, without modulation. Normalized maps were spatially smoothed [8 mm full-width at half-maximum (FWHM) kernel].

Images of change in V_T (ΔV_T) were calculated as: $\Delta V_T = V_T(12\ \text{weeks}) - V_T(\text{baseline})$. These 'delta' images were calculated after within-subject registration of the 12-week parametric map to the baseline map. Delta images were then normalized to MNI space. Similar results were obtained when delta images were computed in MNI space instead. Lesions apparent on T_1 MRI were manually segmented and voxels excluded from all imaging analyses.

Regions of interest were generated from automated volumetric segmentation of T_1 images using Freesurfer (Desikan-Killiany atlas) (Fischl, 2012). Co-registered ^{11}C-PBR28 parametric maps (V_T/DVR) were sampled from regions of interest (cerebral white matter, thalamus and cortical grey matter). To improve sampling accuracy, region of interest masks were intersected with thresholded tissue probability maps ($P > 0.5$). Co-registered ^{11}C-PBR28 parametric maps were sampled from the regions of interest and mean values calculated.

MRI analysis

For cross-sectional voxel-based morphometry (VBM) (Supplementary Fig. 1B), T_1 images were segmented into grey and white matter, and warped to MNI space including modulation by the Jacobian determinants derived from DARTEL. The normalized segmentations were then smoothed (8 mm FWHM) and masked (group mean $P > 0.2$). Total grey and white matter tissue volumes, and intracranial volume, were calculated using SPM12.

Longitudinal volume changes were calculated as follows: (i) annualized change in grey matter and white matter volumes were calculated as: $\%\Delta/\text{year} = ([\text{volume(6-month)}/\text{volume (baseline)}] - 1) \times 100) /$ follow-up interval (years); (ii) an unbiased within-subject pairwise longitudinal registration approach provided a voxelwise measure of change (Ashburner and Ridgway, 2013) (Supplementary Fig. 1C). In SPM12, deformation fields mapping baseline and 6-month T_1s to a within-subject average template T_1 were computed, from which annualized Jacobian determinant images were created, representing the per-year contraction or expansion of each voxel. Within-subject templates were segmented into grey matter and white matter. The segmentations and individual Jacobian determinant images were normalized to MNI space using DARTEL (as above), without modulation, and smoothed (8 mm FWHM). Each Jacobian determinant image was then multiplied by grey matter and white matter tissue segmentation images to yield tissue-specific Jacobian determinant images for voxelwise analysis.

Diffusion-weighted images (Supplementary Fig. 1D) were preprocessed using standard methods (Kinnunen *et al.*, 2011) and tensor-based registration performed using DTI-TK (Zhang *et al.*, 2007). For cross-sectional analysis, normalization of tensor images was performed by bootstrapping subject volumes to the IXI Aging Template then refining the group template using affine followed by non-linear diffeomorphic registration (Zhang *et al.*, 2007). A final study template was registered to MNI space (IIT Human Brain Atlas) using an affine registration step. All subject images were then transformed to MNI space by combining the subject-to-group and group-to-MNI transformations. Maps of fractional anisotropy were generated from normalized tensor images and analysed using tract-based spatial statistics (Kinnunen *et al.*, 2011).

Statistical analysis

Group characteristics were compared using independent sample *t*-tests (for age), Fisher's exact test (gender, *TSPO* genotype) and Mann-Whitney U-tests (time since injury, post-traumatic amnesia duration, visit intervals). Group differences in cognitive performance were assessed using either independent sample *t*-tests or Mann-Whitney U-tests (where data were not normally distributed according to the Shapiro-Wilk test), with Bonferroni multiple comparisons correction.

Voxelwise cross-sectional comparison of ^{11}C-PBR28 DVR, tissue volumes (VBM) and DTI metrics were performed using non-parametric permutation tests (Nichols and Holmes, 2002) in FSL (10 000 permutations). For all analyses, age was added as a nuisance covariate. For comparisons of ^{11}C-PBR28, *TSPO* genotype was included as a covariate and, for VBM analysis, intracranial volume. All results were cluster corrected using threshold-free cluster enhancement (TFCE) (Smith and Nichols, 2009) with family-wise error rate of $P < 0.05$. For ^{11}C-PBR28 region of interest analysis, mean DVR for each region of interest was compared between groups using ANCOVA, with DVR as the dependent variable and genotype and age as covariates, and Fisher LSD *post hoc* tests.

A mean composite processing speed measure for patients was calculated using separate test scores in this domain (Supplementary Table 2) converted to Z-scores with controls as a reference (control Z-score mean = 0 and SD = 1). Positive scores always corresponded to better performance (i.e. faster reaction time).

In patients, partial correlation was used to assess whether DVR in regions of interest with increased binding were associated with time since injury or composite processing speed, with genotype and age as nuisance covariates. Bonferroni correction was used.

Plasma NFL values were log-transformed before group comparison using an independent sample *t*-test. Partial correlation was used to assess whether baseline NFL and the white matter region of interest ^{11}C-PBR28 DVR were associated, with genotype as a nuisance covariate. Spearman's correlation was used to assess association with time since injury, duration of PTA and information processing speed.

To enable direct comparison of modalities, maps of ^{11}C-PBR28 DVR, tissue volumes and DTI metrics were converted to Z-score maps (Z-maps). Z-maps were calculated for each patient and modality, using controls as a reference (control Z-map mean = 0 and SD = 1). To create Z-maps of ^{11}C-PBR28 DVR, adjusted for age and genotype, first a voxelwise regression was performed in FSL on baseline patient and control DVR maps, with age and genotype as covariates. Second, Z-maps for each patient were computed using the voxelwise formula: Z = (patient's residual − mean of residuals in controls) / SD of residuals in controls. A similar procedure was used to create Z-maps of (modulated) tissue volumes (adjusted for age and intracranial volume) and DTI metrics (adjusted for age). All maps were generated from smoothed MNI space images. Then, to directly compare ^{11}C-PBR28 DVR with other modalities within a patient, firstly masks of voxels with 'high' DVR (thresholded at $Z > +2$) and 'normal' DVR ($-1 < Z < +1$) were defined. Then, the two masks were used to sample the Z-maps of the other modalities. The mean Z-scores sampled using high and normal masks were then compared in patients using a paired-sample *t*-test.

Longitudinal changes in tissue volumes were assessed in patients without modelling treatment group. To assess longitudinal changes in total tissue volumes, a one-sample *t*-test was used on %Δ/year measures (above), for grey matter and white matter separately. For longitudinal changes in Jacobian determinant, voxelwise analyses on Jacobian determinant images were performed using one-sample *t*-test ($\Delta > 0, \Delta < 0$) equivalents of non-parametric permutation tests.

Voxelwise differences in baseline ^{11}C-PBR28 binding between treatment groups were assessed using non-parametric permutation tests (as above). Changes in V_T between baseline and 12 weeks in the two groups were first analysed separately using one-sample *t*-test equivalent non-parametric permutation tests on ΔV_T images, with *TSPO* genotype as a nuisance covariate. The two groups were then directly compared using permutation tests, with genotype as a covariate. For region of interest analysis, the effect of minocycline versus no drug on V_T for each region of interest was first assessed using repeated-measures ANOVA, with time as the within-subjects factor (baseline and 12-week) and treatment group (minocycline or no drug) and genotype as between-subjects factors. *Post hoc* tests were planned after significant group × time interactions. $\%\Delta V_T$ and 95% confidence intervals (CI) for each region of interest were calculated in each group and tested for significance using a one-sample *t*-test. A partial correlation assessed whether drug levels were associated with regional ΔV_T, with genotype as a nuisance covariate. The effect of treatment group on change in separate cognitive measures was assessed using repeated-measures ANOVA, as above.

Results

We enrolled 15 patients at least 6 months after a moderate-to-severe TBI (Table 1 and Supplementary Table 1). All patients had one or more focal lesions. None of the patients had undergone neurosurgery.

Microglial activation after traumatic brain injury

At baseline, regions of abnormally high ^{11}C-PBR28 DVR, a local measure of binding normalized to whole brain levels, were found in all of the TBI patients. These were prominent in the white matter (Fig. 2A). A voxelwise contrast of patients versus controls showed significant increases in ^{11}C-PBR28 DVR in frontal and temporal white matter, striatum, thalamus and brainstem in patients (Fig. 2B). Previous studies suggest CMA is prominent in the thalamus and white matter (Ramlackhansingh *et al.*, 2011; Smith *et al.*, 2012; Johnson *et al.*, 2013). Region of interest analysis confirmed this observation. In patients, ^{11}C-PBR28 DVR was increased in cerebral white matter [$F(1,38) = 7.42$, $P = 0.01$, partial $\eta^2 = 0.16$] and thalamus [$F(1,38) = 5.11$, $P = 0.03$, partial $\eta^2 = 0.12$]. No significant difference was seen in the cortical grey matter region of interest.

Cognitive impairment and microglial activation

Patients and controls were well matched on the Wechsler Test of Adult Reading, a test of premorbid intellectual ability (Supplementary Table 2). However, patients showed impairment in a range of cognitive domains, including information processing speed and executive function. Composite processing speed correlated negatively with thalamic ^{11}C-PBR28 DVR in patients ($r = -0.592$, $P = 0.026$), similar to our previous findings (Ramlackhansingh *et al.*, 2011), but was not correlated with white matter DVR.

Microglial activation and axonal injury

VBM of T_1 MRI showed widespread reductions in white matter volume in patients versus controls (Fig. 3A). Grey matter volume was also lower within frontal and temporal cortex, hippocampus and subcortical structures (Fig. 3B). Diffusion MRI showed widespread decreases in fractional anisotropy (Fig. 3C), indicating chronic abnormalities in

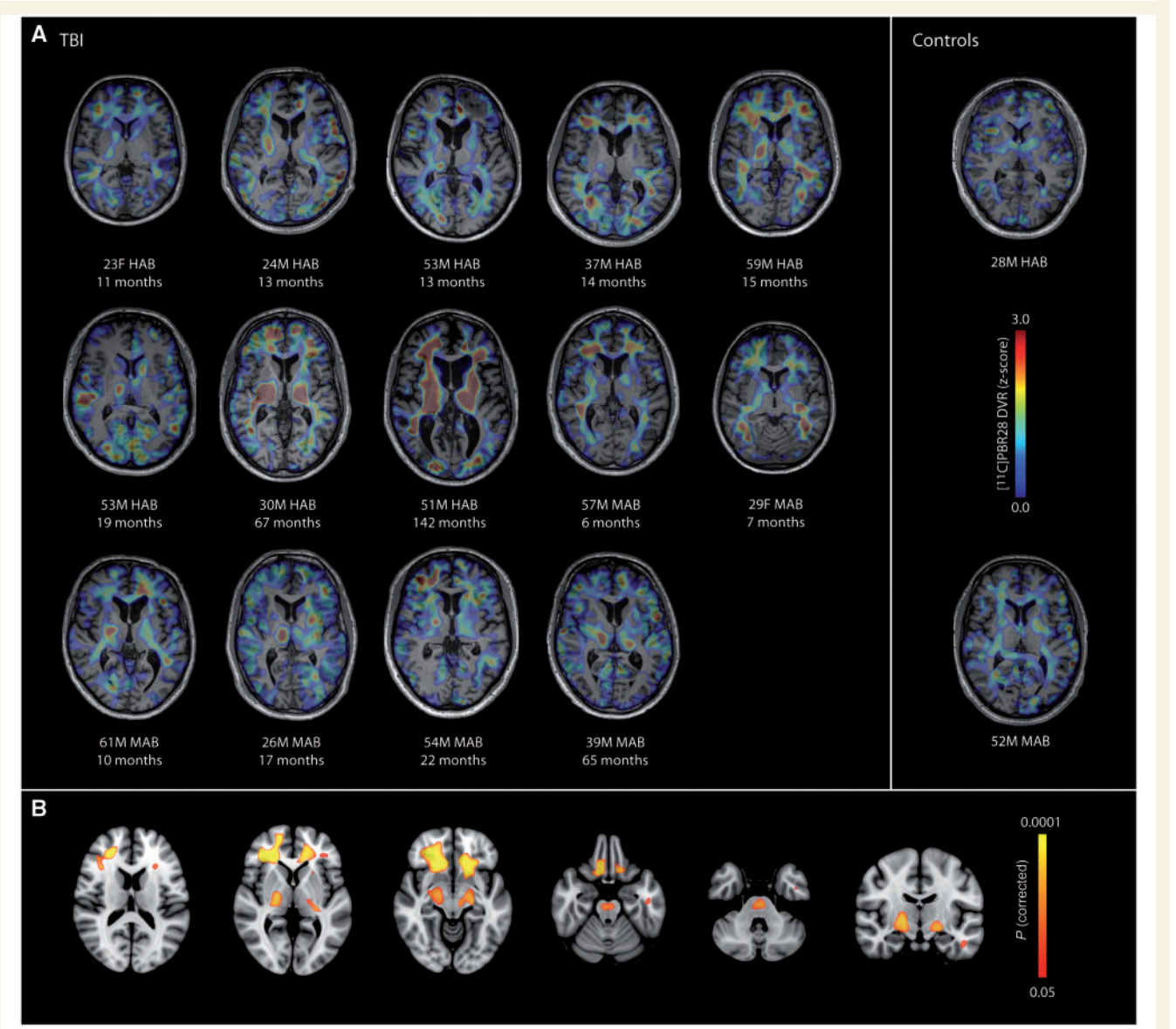

Figure 2 Increased baseline ^{11}C-PBR28 binding in TBI in white matter and subcortical regions. (**A**) Individual standardized (z-score) images of baseline ^{11}C-PBR28 DVR are superimposed on axial T_1 MRIs. Voxels with increased DVR ($z > 0$) compared to the control mean, when controlling for age and *TSPO* genotype, are shown. Baseline images for 14 TBI patients and two representative controls are show. The age (years), gender and TSPO binding class (determined from the *TSPO* genotype) of participants is shown. In patients, the time since injury to baseline scanning is also shown. M = male; F = female; HAB = high affinity binder; MAB = medium affinity binder (Owen *et al.*, 2012). (**B**) Red-yellow areas show significantly increased ^{11}C-PBR28 DVR in patients compared to controls. Results are thresholded using threshold free cluster enhancement (family-wise error correction $P < 0.05$).

white matter tract structure. Regions of volume loss and decreased fractional anisotropy extended far beyond focal lesions (Fig. 3D).

Neuropathological studies suggest CMA co-localizes with white matter damage (Smith *et al.*, 2012; Johnson *et al.*, 2013). Across the whole group, regions showing high baseline ^{11}C-PBR28 DVR in patients (Fig. 2B) overlapped with areas of reduced white matter volume (Fig. 3A) and lower fractional anisotropy (Fig. 3C). Within individual patients, white matter voxels with high ^{11}C-PBR28 DVR showed a greater reduction in tissue volume than those voxels with normal DVR (Fig. 3E) ($P = 0.004$). Similarly, white matter voxels with high DVR also had lower fractional anisotropy than voxels with normal DVR (Fig. 3F) ($P = 0.003$).

Microglial activation and neurodegeneration

In patients, we investigated the relationship between baseline CMA and subsequent neurodegeneration over 6 months using repeated volumetric MRI. Across all patients, total white matter volume decreased significantly between baseline

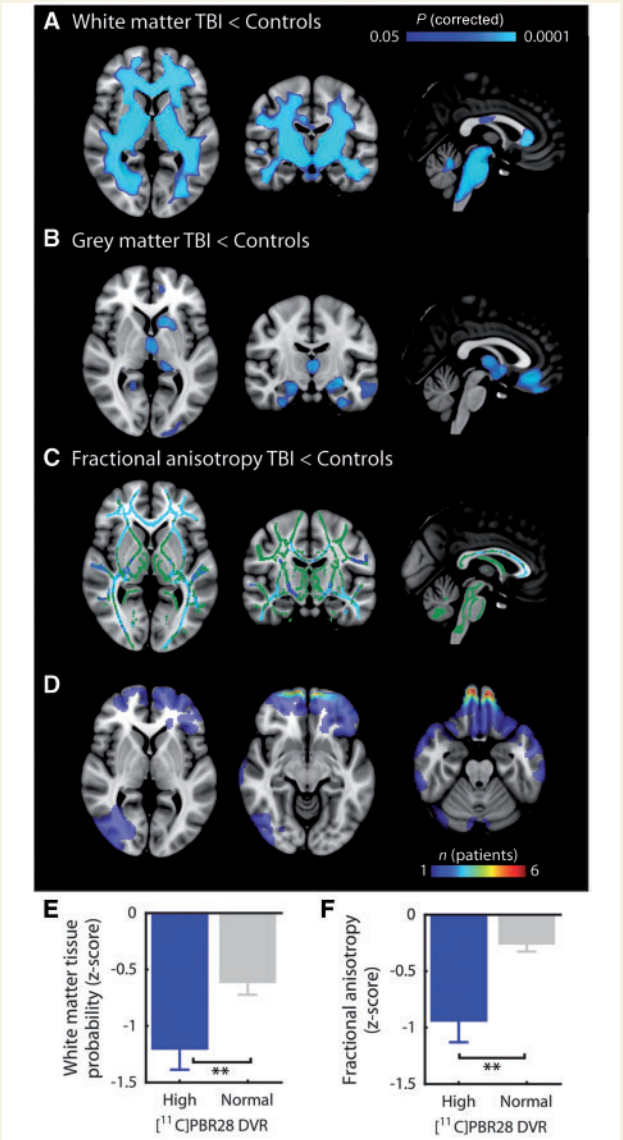

Figure 3 Baseline white matter volume loss and reduced white matter tract structure are greater in areas of high ^{11}C-PBR28 binding in TBI patients. (**A**) Blue–light blue areas show significantly decreased white matter volume loss in patients compared to controls. Results are thresholded using threshold free cluster enhancement (family-wise error correction $P < 0.05$). (**B**) Significantly decreased grey matter volume in patients compared to controls. Thresholding and colour bar are as for **A**. (**C**) Blue–light blue areas show significantly decreased fractional anisotropy in patients compared to controls. The contrast is overlaid on the mean fractional anisotropy skeleton (green). Thresholding and colour bar are as for **A**. (**D**) Overlap map in patients of lesions visible on T_1 structural imaging. The colour of the map indicates the number of patients with a lesion in that area. Maps were computed by summation of the normalized binary lesion masks of individual patients. (**E**) In patients, white matter tissue probability, a measure of tissue volume expressed as a z-score with controls as a reference, is shown for areas of individually-defined high levels of white matter ^{11}C-PBR28 DVR (blue bar) and normal levels of DVR (grey bar). (**F**) As for **E**, but showing fractional anisotropy, expressed as a z-score with controls as a reference. Bars for **E** and **F** are mean ± standard error of the mean (SEM) $^{**}P < 0.01$.

and 6 months (annualized mean ± SD −1.6 ± 2.8% per year, $P = 0.039$, scan interval 0.50 ± 0.07 years). There was no change in total grey matter volume. Controls, followed-up over a longer interval (1.11 ± 0.18 years), showed no change in white matter (0.06 ± 0.77% per year, $P = 0.758$) or grey matter.

White and grey matter contracted over time in patients to variable extents in different brain regions (Fig. 4A). Atrophic changes (Jacobian determinant < 0) were seen in frontal and subcortical white matter (Fig. 4B), as well as frontal, temporal and subcortical grey matter (Fig. 4C). No significant changes in Jacobian determinant were detected in controls. In patients, the mean Jacobian determinant in white matter voxels with high baseline ^{11}C-PBR28 DVR was more negative than those voxels with normal baseline DVR ($P = 0.004$), indicating that parts of the white matter with high CMA at baseline underwent greater atrophy over the subsequent 6 months (Fig. 4D).

Neurofilament light chain and microglial activation

Plasma NFL provided a measure of active neurodegeneration. Baseline NFL levels were higher in patients than controls (Fig. 5A) (t = 3.09, $P = 0.007$). Levels were negatively correlated with time since injury (r = −0.546, $P = 0.035$), but 11/15 patients had elevated levels compared to controls (Fig. 5B). Baseline NFL levels were positively correlated with ^{11}C-PBR28 DVR in cerebral white matter (Fig. 5C) (r = 0.519, $P = 0.042$). In contrast, there was no correlation between NFL and duration of post-traumatic amnesia, an indicator of original injury severity (r = −0.268, $P = 0.377$), nor between NFL and composite processing speed.

Minocycline reduces microglial activation

We next investigated the effect of 12 weeks of minocycline treatment on ^{11}C-PBR28 binding in the TBI patients. One group ($n = 10$) received minocycline 100 mg orally twice daily for 12 weeks; the other ($n = 5$) had no drug (Fig. 1). Baseline characteristics and cognitive performance were similar between minocycline and untreated groups (Table 2, Supplementary Tables 1 and 2).

The ^{11}C-PBR28 V_T, which provides an absolute measure of uptake (Jucaite *et al.*, 2015; Sandiego *et al.*, 2015), was used as the outcome measure for assessing within-subject drug effects. Voxel-wise changes in V_T between baseline and 12 weeks (ΔV_T) were first analysed in the minocycline and untreated groups separately (Fig. 6A and B). There were no significant baseline differences in V_T between the two groups. In the minocycline group, ^{11}C-PBR28 V_T was reduced at 12 weeks compared to baseline across most brain regions (Fig. 6B). V_T in the untreated patients over the same period did not change (Fig. 6B). V_T reductions in most of the parenchyma were seen after minocycline

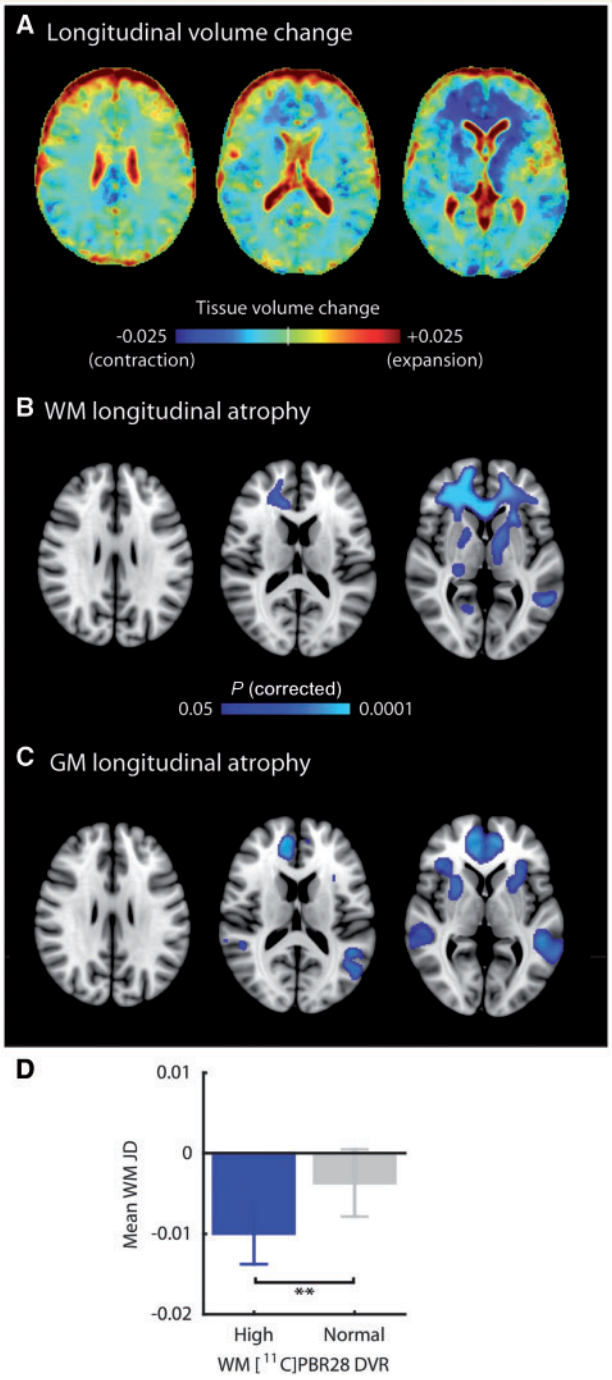

Figure 4 Longitudinal white matter atrophy over 6 months in TBI patients is greater in areas of high baseline ^{11}C-PBR28 binding. (**A**) Mean annualized Jacobian determinant (JD) images, indexing longitudinal change over 6 months in patients. Green colours represent little or no change over time, yellow-red colours reflect volumetric increases (expansion, positive Jacobian determinant), while blue–light blue colours reflect volumetric decreases (contraction, negative Jacobian determinant). Mean Jacobian determinant images are superimposed on the MNI T_1 template. (**B**) Blue–light blue areas show significantly decreased Jacobian determinant, indicating longitudinal atrophy in white matter (WM) over 6 months (white matter tissue-specific Jacobian determinant < 0), in patients. Results are thresholded using threshold free cluster enhancement (family-wise error correction < 0.05).

treatment when ΔV_T was compared across the two groups (Fig. 6C).

Region of interest analysis showed that minocycline reduced V_T compared to baseline in the cerebral white matter region of interest by $-23.30 \pm 19.09\%$ (mean $\pm$ SD) (95% CI -40.9 to -5.64%, $P = 0.018$), the thalamus ($-24.18 \pm 18.71\%$, CI -41.48 to -6.90%, $P = 0.014$) and cortical grey matter ($-22.05 \pm 19.33\%$, CI -39.93% to -4.17%, $P = 0.023$) (Fig. 6D). There were no significant changes in the untreated group.

A region of interest analysis of cerebral white matter showed a significant treatment group $\times$ time interaction [$F(1,9) = 7.178$, $P = 0.025$, partial $\eta^2 = 0.444$], with non-significant effects of group, time, genotype and genotype $\times$ time. *Post hoc* Fisher LSD tests explain this as arising from a V_T reduction between baseline and 12 weeks in the minocycline group (mean difference $\pm$ standard error -0.741 ± 0.190, $P = 0.004$, 95% CI -1.171 to -0.311) but no change in the no drug group (-0.048 ± 0.225, $P = 0.835$, 95% CI -0.557 to 0.461). Analysis of the thalamus region of interest showed a similar significant group $\times$ time interaction [$F(1,9) = 7.569$, $P = 0.022$, partial $\eta^2 = 0.457$, mean difference $\pm$ standard error in the minocycline group -1.097 ± 0.310, $P = 0.006$, 95% CI -1.798 to -0.395], as well as cortical grey matter [$F(1,9) = 6.255$, $P = 0.034$, partial $\eta^2 = 0.410$, mean difference $\pm$ standard error -0.855 ± 0.245, $P = 0.007$, 95% CI -1.408 to -0.301].

Compliance with minocycline dosing (defined as the proportion of expected number of tablets taken) was $91 \pm 10\%$ (mean $\pm$ SD, range 73–99%). Plasma trough minocycline levels at 12 weeks were 2.08 ± 0.55 mg/l (mean $\pm$ SD, range 1.29–2.80 mg/l). There was no significant correlation between drug trough levels or compliance with dosing and ΔV_T in any of the three regions of interest.

Minocycline, neurofilament light chain and neurodegeneration

Plasma NFL levels increased after 12 weeks of minocycline compared to the untreated group, then returned to baseline levels at 6 months, after drug discontinuation (Fig. 6E). Repeated-measures ANOVA showed a significant treatment arm $\times$ time interaction [$F(2,22) = 6.155$, $P = 0.008$, partial $\eta^2 = 0.359$]. *Post hoc* Fisher LSD tests showed a NFL

Figure 4 Continued
(**C**) Regions of significantly decreased Jacobian determinant in grey matter (GM) over 6 months in patients, indicating longitudinal atrophy inn grey matter (grey matter tissue-specific Jacobian determinant < 0). Thresholding and colour bar are as for **B**. (**D**) In patients, mean Jacobian determinant in white matter is shown for areas of individually-defined high levels of white matter ^{11}C-PBR28 binding (distribution volume ratio, DVR) (blue bar) and normal levels of DVR (grey bar). Bars are mean $\pm$ SEM $^{**}P < 0.01$.

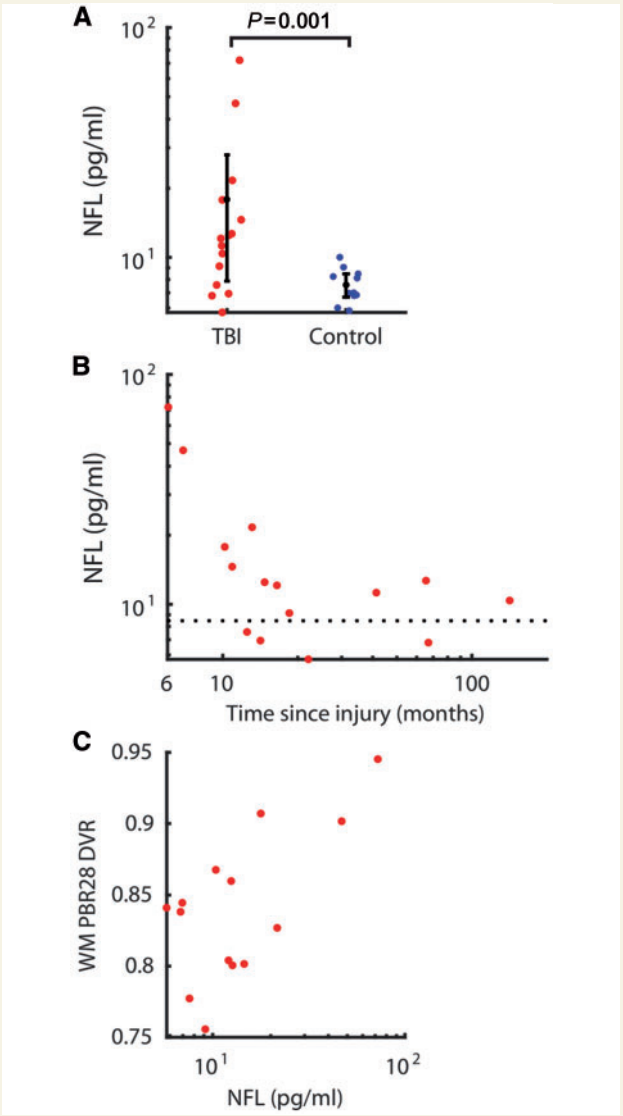

Figure 5 Plasma NFL and associations with ^{11}C-PBR28 white matter binding and time since injury. (**A**) Plasma NFL levels are shown for TBI patients (red dots) and controls (blue dots). Black bars show mean and 95% confidence intervals. Note *y*-axis is logarithmic. (**B**) Plasma NFL in TBI patients (*y*-axis) is plotted against time since injury in months (*x*-axis). Dotted horizontal line indicates upper limit of 95% confidence interval in controls. Note both axes are logarithmic. (**C**) ^{11}C-PBR28 DVR of the cerebral white matter (WM) region of interest in TBI patients (*y*-axis) plotted against plasma NFL level (*x*-axis, logarithmic).

increase between baseline and 12 weeks in the minocycline group (mean difference ± standard error 0.386 ± 0.093, 95% CI 0.182 to 0.591), but no significant change in the untreated group (−0.0687 ± 0.125, 95% CI −0.343 to 0.209).

Across all patients, change in NFL was negatively correlated with change in white matter ^{11}C-PBR28 V_T ($r = -0.558$, $P = 0.048$) (Fig. 6F). Baseline NFL negatively correlated with mean Jacobian determinant over 6 months ($r = -0.562$, $P = 0.005$) (Fig. 6G), with a strong correlation seen in the minocycline arm ($r = -0.850$, $P = 0.004$).

Side effects of minocycline

Minocycline treatment was generally well-tolerated in patients. One patient had mild nausea and vomiting, which was treated initially with anti-emetics and resolved after reducing the minocycline dose to 100 mg once daily. One patient had mild subjective unilateral hearing impairment, which began within days of starting minocycline. This was treated initially with decongestants and resolved spontaneously despite continuation of the minocycline.

Discussion

We found CMA after moderate-severe TBI was associated with white matter damage months and years after injury. Areas with higher CMA showed greater progressive atrophy. The antibiotic minocycline reduced microglial activation but increased levels of plasma NFL, a marker of axonal injury and neurodegeneration. These findings suggest that microglial activation has a reparative effect in the chronic phase of TBI.

Increased ^{11}C-PBR28 binding was seen in damaged and progressively atrophying white matter. This extended our previous observation of microglial activation in the thalamus and white matter using another TSPO PET ligand, ^{11}C-PK11195 (Ramlackhansingh *et al.*, 2011). Microglia might be chronically stimulated by the persistence of myelin breakdown products from the initial injury (Johnson *et al.*, 2013; Faden and Loane, 2015), but TSPO PET alone does not clarify their functional effects. Microglial function *in vivo* is heterogeneous and can involve pro-inflammatory and reparative activation phenotypes (Holmin and Mathiesen, 1999; Nagamoto-Combs *et al.*, 2007, 2010; Loane *et al.*, 2014; Ransohoff, 2016). Therefore, depending on the functional phenotype, inhibiting microglia with minocycline would be expected to have distinct effects. Experimental animal work has not clarified this issue, as evidence exists for both damaging and reparative phenotypes in the months after injury (Holmin and Mathiesen, 1999; Nagamoto-Combs *et al.*, 2007, 2010; Loane *et al.*, 2014), and the function of activated cells is likely to change over time (Kumar *et al.*, 2016). Hence, CMA might be either damaging or reparative in the chronic phase. Our findings suggest the latter, because NFL increased following minocycline treatment that dramatically reduced ^{11}C-PBR28 binding. However, because the time course of microglial activation phenotype evolves after injury, minocycline treatment at an earlier time point may well produce different effects. Hence, drug treatment may need to be targeted to the dominant microglial phenotype at a specific time since injury, rather than simply attempting to inhibit microglial activation. In addition, the cross-sectional

Table 2 Baseline characteristics of the two TBI patient treatment groups

	TBI Minocycline	TBI No drug	*P*-value
n	10	5	-
Age, years	41.7 ± 15.0	43.4 ± 12.3	0.831
Gender, *n* male/%	9/90	4/80	0.571
Genotype, *n* HABs/%	6/60	3/60	0.713
Time since injury, months (IQR)	17.5 (37.0)	14.1 (30.2)	0.573
Duration of PTA, days (IQR)	4 (46)	8.5 (17)	0.511

Numerical values for age are mean ± SD. Numerical values for time since injury and post-traumatic amnesia (PTA) are median (IQR). HABs = high-affinity binders.

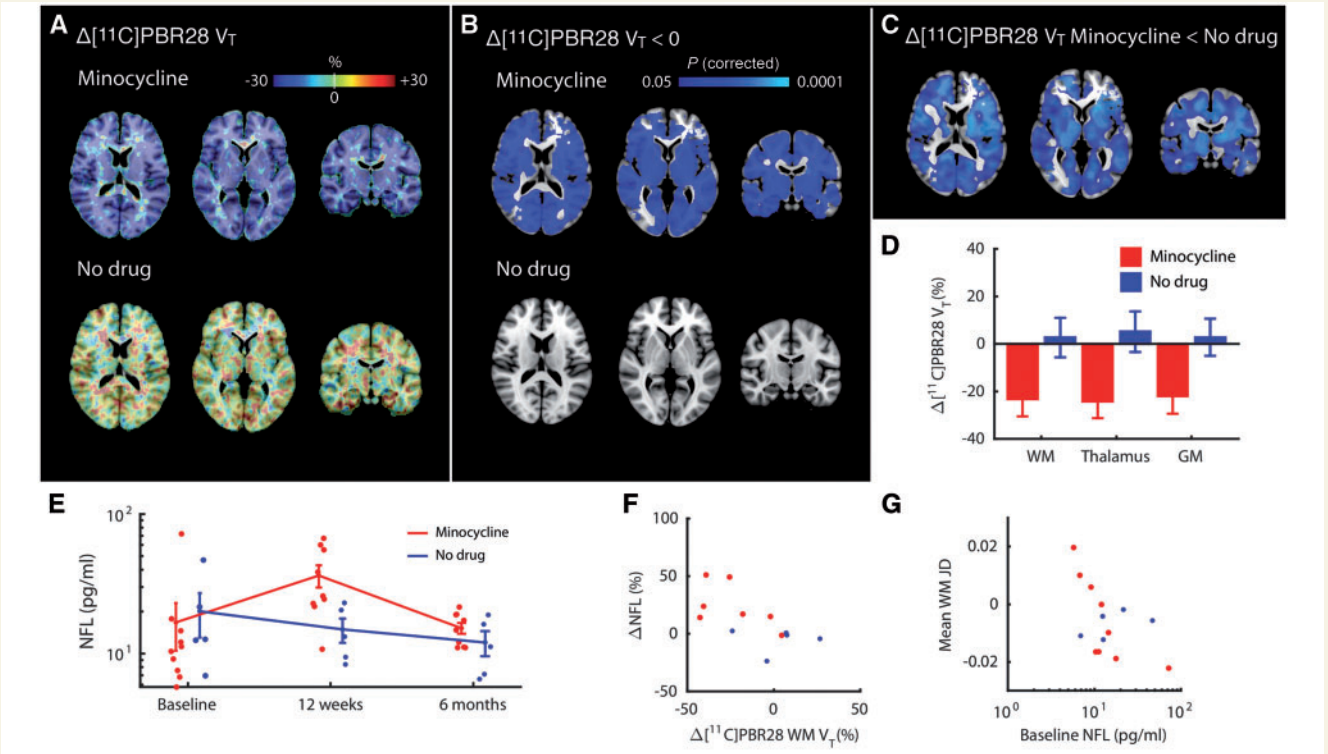

Figure 6 Effect of minocycline treatment in TBI patients on ^{11}C-PBR28 binding, plasma NFL and longitudinal atrophy. (**A**) Mean change in ^{11}C-PBR28 volume of distribution (ΔV_T) between baseline and 12-week visits, expressed as a percentage of baseline V_T, in patients who received minocycline treatment (*n* = 7) (*top row*) and no drug (*n* = 5) (*bottom row*). See Fig. 1 for description of excluded data. Green colours represent little or no change over time, yellow-red colours reflect V_T increases over time, while blue-light blue colours reflect V_T decreases. Images are superimposed on the MNI T_1 template. (**B**) Blue-light blue areas show significantly decreased V_T between baseline and 12-week visits ($\Delta V_T < 0$), in patients who received minocycline treatment (*top row*) and no drug (bottom row). Results are thresholded using threshold free cluster enhancement (family-wise error correction < 0.05). Neither group showed areas of significantly increased V_T ($\Delta V_T > 0$). (**C**) Blue-light blue areas show significantly reduced ΔV_T in patients who received minocycline treatment compared to patients who received no drug. There were no areas of significantly increased ΔV_T. Thresholding and colour bar are as for **B**. (**D**) Mean ± SEM group change in V_T, expressed as a percentage of baseline V_T, in patients who received minocycline treatment (blue bars) and no drug (red bars), in white matter (WM), thalamus and cortical grey matter (GM) regions of interest. (**E**) Plasma NFL levels are shown for TBI patients treated with minocycline (red dots) and untreated patients (no drug, blue dots) for the three visits. Bars show visit mean (connected over time) and standard error. Note *y*-axis is logarithmic. (**F**) Percentage change in NFL between baseline and 12 weeks (*y*-axis) is plotted against percentage change in white matter ^{11}C-PBR28 VT (*x*-axis) measured over the same period. Colours are defined as in **E**. (**G**) Mean white matter Jacobian determinant (JD, *y*-axis) (measured between baseline and 6 months) is plotted against baseline NFL in patients.

PET findings may also have differed in a patient cohort studied closer to the time of injury.

Our results suggest that inhibition of CMA after TBI promotes neurodegeneration. Plasma NFL is highly correlated with CSF NFL (Lu *et al.*, 2015; Gisslén *et al.*, 2016; Shahim *et al.*, 2016; Hansson *et al.*, 2017), and elevations in plasma NFL have been observed in a variety of neurodegenerative diseases, including Alzheimer's disease and amyotrophic

lateral sclerosis (Gaiottino *et al.*, 2013; Lu *et al.*, 2015; Bacioglu *et al.*, 2016*b*; Gisslén *et al.*, 2016). Here we show that plasma NFL is elevated in the chronic phase after moderate–severe TBI, and that plasma levels of NFL increased significantly after 12 weeks of minocycline treatment, before returning to baseline after stopping the drug. A direct relationship between CMA and NFL is made more likely by the negative correlation observed between changes in ^{11}C-PBR28 binding and NFL levels. In addition, the link between NFL and progressive neurodegeneration is strengthened by the presence of a negative correlation between baseline NFL and longitudinal atrophy, such that higher baseline NFL predicted greater white matter atrophy over the subsequent 6 months.

Studies in non-human primates suggest a trophic role for CMA after TBI, which may explain our observations (Nagamoto-Combs *et al.*, 2007, 2010). Long-term follow-up in a primate model of TBI confirmed the presence of persistent microglial activation up to 12 months after injury, which was associated with expression of factors that support cell survival, including BDNF and ERK1/2. In contrast, TNF-α, IL-1β and IL-6 expression were reduced months after injury, suggesting that the more immediate pro-inflammatory response had subsided. In a primate spinal cord injury model, microglial activation was observed at sites of synaptic sprouting, suggesting a role in promoting axonal regeneration after TBI (Nagamoto-Combs *et al.*, 2010).

Although effects of minocycline on microglia have been demonstrated *in vitro* and in preclinical models (Garrido-Mesa *et al.*, 2013*a*), ours is the first study to demonstrate directly that standard clinical doses of 200 mg/day provide an adequate CNS concentration to inhibit microglial activation in the brain. Animal studies have typically used much higher doses (equivalent by weight to ~3–7 g/day in humans), which are likely to be toxic in humans (Plane *et al.*, 2010). The reduction in ^{11}C-PBR28 binding provides evidence that the standard clinical dose has a pharmacodynamic action on humans comparable to the ~50% reduction in microglial activation seen following administration of pharmacological doses to mice after experimental TBI (Homsi *et al.*, 2010). Here we show a ~25% reduction in ^{11}C-PBR28 V_T after minocycline. If activated microglia accounted for all of the displaceable TSPO binding, this suggests a ~50% reduction in activated microglia, once the non-specific element of ^{11}C-PBR28 binding has been accounted for (Owen *et al.*, 2014).

Clinical studies of minocycline in other neurological conditions have reported varying results. Two stroke trials showed improved motor outcomes following minocycline treatment in the acute phase (Lampl *et al.*, 2007; Padma Srivastava *et al.*, 2012). However, the largest neurological study of minocycline showed an adverse effect on the progression of patients with amyotrophic lateral sclerosis (Gordon *et al.*, 2007), a condition in which elevated NFL is a poor prognostic indicator (Lu *et al.*, 2015). Minocycline was found to have detrimental effects on functional rating scores in a dose-independent manner (Gordon *et al.*, 2007), suggesting that microglia could have a net reparative phenotype and that inhibition accelerated neurodegeneration. It is also possible that the disparate clinical effects of minocycline are mediated through mechanisms other than microglial modulation.

There are a number of potential limitations to our study. First, we powered our study for ^{11}C-PBR28, which resulted in sample sizes too small for the assessment of some other outcome measures. This is particularly true for clinical measures of the drug effect, which we have not reported because of this issue. A much larger clinical trial would be required to study the clinical effects of minocycline, but our results suggest that this would be inappropriate if the aim is to reduce long-term neurodegenerative effects of CMA. A larger sample size may also permit exploration of other effects on microglial activation and neurodegeneration, such as gender, age and genetic factors. Second, the study was open label, so investigators were not blinded to an individual's treatment. However, this is unlikely to have affected our objective neuroimaging and fluid biomarker outcome measures, and is mitigated by the repeat assessment of patients following drug cessation. We have focused on the effects of minocycline on microglia, but the drug is known to have a broad range of actions (Garrido-Mesa *et al.*, 2013*b*). This potentially complicates the interpretation of our NFL findings, but our results suggest that an effect of the drug on white matter microglia is linked to the increase in plasma NFL seen after treatment. It will be important for future human and basic science work to investigate the causative links between CMA and neurodegeneration measured using markers such as NFL. Analysis of cytokines in blood, in parallel with NFL measurements, may have helped to explain the action of minocycline. However, whilst a recent review of methods to measure neuroinflammation after brain injury highlights some studies linking blood cytokines and functional outcomes (Thelin *et al.*, 2017), peripheral blood markers that directly track microglial function are not established. Finally, our patients had focal lesions, which could potentially have affected our neuroimaging analyses. However, to control for the possible effects of lesions, we excluded lesioned areas from the analysis. Here and in our previous work using ^{11}C-PK11195 we found binding was reduced in visible lesions, which would have biased the analysis against detecting increases.

Several of our results are potentially clinically important. We have demonstrated CMA accompanying markers of progressive damage following brain trauma. These findings highlight that TBI is not a static insult, but rather a chronic, progressive neurodegenerative disease. Many TBI survivors make a poor recovery or deteriorate long after the injury, but it is not currently possible to identify patients who are likely to do so. A biomarker of disease progression would allow patients at risk of poor outcomes to be identified, and would facilitate clinical studies of long-term sequelae of TBI. Our results suggest that combining

plasma NFL and neuroimaging measures of progressive white matter atrophy may be a promising approach. This may have clinical utility, for example, in quantifying the accumulated brain injury sustained as a result of multiple mild TBIs, such as during a professional sporting career, and estimating the risk of developing post-traumatic dementia, including chronic traumatic encephalopathy (McKee *et al.*, 2013). Finally, our results suggest that there may be positive effects of chronic microglial activation after TBI, and that promoting a trophic phenotype for microglia may improve the recovery of damaged axons.

Acknowledgements

We thank the subjects who took part in the study. We thank the staff at the Imanova Centre for Imaging Sciences, London, the Clinical Imaging Facility, Imperial College London, the Clinical Neurochemistry Laboratory in Mölndal, Sweden, and the Antimicrobial Reference Laboratory, Southmead Hospital, Bristol.

Funding

G.S. was supported by a clinical research fellowship awarded in the Wellcome Trust-GlaxoSmithKline Translational Medicine Training Programme. D.R.O. is supported by the UK National Institute for Health Research (NIHR). P.M.M. has research support from the MS Society of Great Britain, the Progressive MS Alliance, the Medical Research Council (MRC) and GlaxoSmithKline and personal support from the Edmund J. Safra Foundation and from Lily Safra. D.J.S. currently holds a National Institute of Health Research Professorship - RP-011-048. K.B. currently holds the Torsten Söderberg Professorship in Medicine. H.Z. is a Wallenberg Academy Fellow. This work was supported by the Imperial College Healthcare Trust Biomedical Research Centre, the Swedish Research Council, the Knut and Alice Wallenberg Foundation, VINNOVA and the Torsten Söderberg foundation. This paper presents independent research funded by the NIHR and carried out at the NIHR/Wellcome Trust Imperial Clinical Research Facility. The views expressed are those of the author(s) and not necessarily those of the NIHR, the NHS or the Department of Health.

Supplementary material

Supplementary material is available at *Brain* online.

References

Annegers JF, Hauser WA, Coan SP, Rocca WA. A population-based study of seizures after traumatic brain injuries. N Engl J Med 1998; 338: 20–4.

Ashburner J. A fast diffeomorphic image registration algorithm. Neuroimage 2007; 38: 95–113.

Ashburner J, Ridgway GR. Symmetric diffeomorphic modelling of longitudinal structural MRI. Front Neurosci 2013; 6: 197.

Bacioglu M, Maia LF, Preische O, Schelle J, Apel A, Kaeser SA, et al. Neurofilament light chain in blood and CSF as marker of disease progression in mouse models and in neurodegenerative diseases. Neuron 2016a; 91: 494–6.

Bacioglu M, Maia LF, Preische O, Schelle J, Apel A, Kaeser SA, et al. Neurofilament light: a dynamic cross-disease fluid biomarker for neurodegeneration. Neuron 2016b; 91: 1–3.

Casha S, Zygun D, McGowan MD, Bains I, Yong VW, Hurlbert RJ. Results of a phase II placebo-controlled randomized trial of minocycline in acute spinal cord injury. Brain 2012; 135: 1224–36.

Cole JH, Leech R, Sharp DJ, for the Alzheimer's disease neuroimaging I. Prediction of brain age suggests accelerated atrophy after traumatic brain injury. Ann Neurol 2015; 77: 571–81.

Faden AI, Loane DJ. Chronic neurodegeneration after traumatic brain injury: Alzheimer disease, chronic traumatic encephalopathy, or persistent neuroinflammation? Neurotherapeutics 2015; 12: 143–50.

Fischl B. FreeSurfer. Neuroimage 2012; 62: 774–81.

Gaiottino J, Norgren N, Dobson R, Topping J, Nissim A, Malaspina A, et al. Increased neurofilament light chain blood levels in neurodegenerative neurological diseases. PLoS One 2013; 8: e75091.

Garrido-Mesa N, Zarzuelo A, Gálvez J. What is behind the non-antibiotic properties of minocycline? Pharmacol Res 2013a; 67: 18–30.

Garrido-Mesa N, Zarzuelo A, Gálvez J. Minocycline: far beyond an antibiotic. Br J Pharmacol 2013b; 169: 337–52.

Gentleman SM. Review: microglia in protein aggregation disorders: friend or foe? Neuropathol Appl Neurobiol 2013; 39: 45–50.

Gisslén M, Price RW, Andreasson U, Norgren N, Nilsson S, Hagberg L, et al. Plasma concentration of the neurofilament light protein (NFL) is a biomarker of CNS injury in HIV infection: a cross-sectional study. EBioMedicine 2016; 3: 135–40.

Gordon PH, Moore DH, Miller RG, Florence JM, Verheijde JL, Doorish C, et al. Efficacy of minocycline in patients with amyotrophic lateral sclerosis: a phase III randomised trial. Lancet Neurol 2007; 6: 1045–53.

Hansson O, Janelidze S, Hall S, Magdalinou N, Lees AJ, Andreasson U, et al. Blood-based NfL A biomarker for differential diagnosis of parkinsonian disorder. Neurology 2017; 88: 930–7.

Holmin S, Mathiesen T. Long-term intracerebral inflammatory response after experimental focal brain injury in rat. Neuroreport 1999; 10: 1889–91.

Homsi S, Piaggio T, Croci N, Noble F, Plotkine M, Marchand-Leroux C, et al. Blockade of acute microglial activation by minocycline promotes neuroprotection and reduces locomotor hyperactivity after closed head injury in mice: a twelve-week follow-up study. J Neurotrauma 2010; 27: 911–21.

Johnson VE, Stewart JE, Begbie FD, Trojanowski JQ, Smith DH, Stewart W. Inflammation and white matter degeneration persist for years after a single traumatic brain injury. Brain 2013; 136: 28–42.

Jucaite A, Svenningsson P, Rinne JO, Cselenyi Z, Varnas K, Johnstrom P, et al. Effect of the myeloperoxidase inhibitor AZD3241 on microglia: a PET study in Parkinson's disease. Brain 2015; 138: 2687–700.

Kinnunen KM, Greenwood R, Powell JH, Leech R, Hawkins PC, Bonnelle V, et al. White matter damage and cognitive impairment after traumatic brain injury. Brain 2011; 134: 449–63.

Kuhle J, Barro C, Andreasson U, Derfuss T, Lindberg R, Sandelius Å, et al. Comparison of three analytical platforms for quantification of the neurofilament light chain in blood samples: ELISA, electrochemiluminescence immunoassay and Simoa. Clin Chem Lab Med 2016; 54: 1655–61.

Kumar A, Alvarez-Croda D-M, Stoica BA, Faden AI, Loane DJ. Microglial/macrophage polarization dynamics following traumatic brain injury. J. Neurotrauma 2016; 33; 1732–50.

Lampl Y, Boaz M, Gilad R, Lorberboym M, Dabby R, Rapoport A, et al. Minocycline treatment in acute stroke an open-label, evaluator-blinded study. Neurology 2007; 69: 1404–10.

Ljungqvist J, Zetterberg H, Mitsis M, Blennow K, Skoglund T. Serum neurofilament light protein as a marker for diffuse axonal injury: results from a case series study. J Neurotrauma 2017; 34: 1124–7.

Loane DJ, Kumar A, Stoica BA, Cabatbat R, Faden AI. Progressive neurodegeneration after experimental brain trauma: association with chronic microglial activation. J Neuropathol Exp Neurol 2014; 73: 14–29.

Logan J, Fowler JS, Volkow ND, Wolf AP, Dewey SL, Schlyer DJ, et al. Graphical analysis of reversible radioligand binding from time-activity measurements applied to [N-11C-methyl]-(-)-cocaine PET studies in human subjects. J Cereb Blood Flow Metab 1990; 10: 740–7.

Loggia ML, Chonde DB, Akeju O, Arabasz G, Catana C, Edwards RR, et al. Evidence for brain glial activation in chronic pain patients. Brain 2015; 138: 604–15.

Lu C-H, Macdonald-Wallis C, Gray E, Pearce N, Petzold A, Norgren N, et al. Neurofilament light chain: a prognostic biomarker in amyotrophic lateral sclerosis. Neurology 2015; 84: 2247–57.

Maas AI, Marmarou A, Murray GD, Steyerberg EW. Clinical trials in traumatic brain injury: current problems and future solutions. Acta Neurochir Suppl 2004; 89: 113–18.

Malec JF, Brown AW, Leibson CL, Flaada JT, Mandrekar JN, Diehl NN, et al. The mayo classification system for traumatic brain injury severity. J Neurotrauma 2007; 24: 1417–24.

McKee AC, Stern RA, Nowinski CJ, Stein TD, Alvarez VE, Daneshvar DH, et al. The spectrum of disease in chronic traumatic encephalopathy. Brain 2013; 136: 43–64.

Nagamoto-Combs K, McNeal DW, Morecraft RJ, Combs CK. Prolonged microgliosis in the rhesus monkey central nervous system after traumatic brain injury. J Neurotrauma 2007; 24: 1719–42.

Nagamoto-Combs K, Morecraft RJ, Darling WG, Combs CK. Long-term gliosis and molecular changes in the cervical spinal cord of the rhesus monkey after traumatic brain injury. J Neurotrauma 2010; 27: 565–85.

Nichols TE, Holmes AP. Nonparametric permutation tests for functional neuroimaging: a primer with examples. Hum Brain Mapp 2002; 15: 1–25.

Owen DR, Guo Q, Kalk NJ, Colasanti A, Kalogiannopoulou D, Dimber R, et al. Determination of [(11)C]PBR28 binding potential *in vivo*: a first human TSPO blocking study. J Cereb Blood Flow Metab 2014; 34: 989–94.

Owen DR, Yeo AJ, Gunn RN, Song K, Wadsworth G, Lewis A, et al. An 18-kDa translocator protein (TSPO) polymorphism explains differences in binding affinity of the PET radioligand PBR28. J Cereb Blood Flow Metab 2012; 32: 1–5.

Padma Srivastava MV, Bhasin A, Bhatia R, Garg A, Gaikwad S, Prasad K, et al. Efficacy of minocycline in acute ischemic stroke: a single-blinded, placebo-controlled trial. Neurol India 2012; 60: 23–8.

Plane JM, Shen Y, Pleasure DE, Deng W. Prospects for minocycline neuroprotection. Arch Neurol 2010; 67: 1442–8.

Raghavendra Rao VL, Dogan A, Bowen KK, Dempsey RJ. Traumatic brain injury leads to increased expression of peripheral-type benzodiazepine receptors, neuronal death, and activation of astrocytes and microglia in rat thalamus. Exp Neurol 2000; 161: 102–14.

Ramlackhansingh AF, Brooks DJ, Greenwood RJ, Bose SK, Turkheimer FE, Kinnunen KM, et al. Inflammation after trauma: microglial activation and traumatic brain injury. Ann Neurol 2011; 70: 374–83.

Ransohoff RM. A polarizing question: do M1 and M2 microglia exist? Nat Neurosci 2016; 19: 987–91.

Sandiego CM, Gallezot J-D, Pittman B, Nabulsi N, Lim K, Lin S-F, et al. Imaging robust microglial activation after lipopolysaccharide administration in humans with PET. Proc Natl Acad Sci USA 2015; 112: 12468–73.

Shahim P, Gren M, Liman V, Andreasson U, Norgren N, Tegner Y, et al. Serum neurofilament light protein predicts clinical outcome in traumatic brain injury. Sci Rep 2016; 6: 36791.

Sidaros A, Skimminge A, Liptrot MG, Sidaros K, Engberg AW, Herning M, et al. Long-term global and regional brain volume changes following severe traumatic brain injury: a longitudinal study with clinical correlates. Neuroimage 2009; 44: 1–8.

Siopi E, Cho AH, Homsi S, Croci N, Plotkine M, Marchand-Leroux C, et al. Minocycline restores sAPP alpha levels and reduces the late histopathological consequences of traumatic brain injury in mice. J Neurotrauma 2011; 28: 2135–43.

Smith C, Gentleman SM, Leclercq PD, Murray LS, Griffin WST, Graham DI, et al. The neuroinflammatory response in humans after traumatic brain injury. Neuropathol Appl Neurobiol 2012; 39: 654–66.

Smith DH, Johnson VE, Stewart W. Chronic neuropathologies of single and repetitive TBI: substrates of dementia? Nat Rev Neurol 2013; 9: 211–21.

Smith SM, Nichols TE. Threshold-free cluster enhancement: addressing problems of smoothing, threshold dependence and localisation in cluster inference. Neuroimage 2009; 44: 83–98.

Thelin EP, Tajsic T, Zeiler FA, Menon DK, Hutchinson PJA, Carpenter KLH, et al. Monitoring the neuroinflammatory response following acute brain injury. Front Neurol 2017; 8: 351.

Whitnall L, McMillan TM, Murray GD, Teasdale GM. Disability in young people and adults after head injury: 5-7 year follow up of a prospective cohort study. JNNP 2006; 77: 640–5.

Zhang H, Avants BB, Yushkevich PA, Woo JH, Wang S, McCluskey LF, et al. High-Dimensional spatial normalization of diffusion tensor images improves the detection of white matter differences: an example study using amyotrophic lateral sclerosis. Med Imaging IEEE Trans 2007; 26: 1585–97.